# B1-Gradient based MRI using a Multi-element Transmit System

**U. Katscher[1], J. Lisinski[2], P. Boernert[1], and I. Graesslin[1]**

[1]Philips Research Laboratories, Hamburg, Germany, [2]University of Applied Sciences, Hamburg, Germany

***Introduction:***
Spatial signal encoding in MRI is usually performed via $B_0$-gradients. An alternative method is the use of $B_1$-gradients (so-called RF encoding), already suggested in the early days of MR (see, e.g., [1-3]). RF encoding offers the possibility to omit all $B_0$-gradients, which would allow for MR scanning more or less free of acoustic noise. This advantage might be counterbalanced by long scan times, long reconstruction times, reduced image contrast, and/or enhanced SAR. This study investigates the principle possibility of RF encoding using an eight-channel whole-body transmit system [4] for low-resolution imaging of phantoms. Future studies can combine $B_0$ and $B_1$-gradients, alleviating the advantages and disadvantages of RF encoding.

***Theory:***
Image acquisition via RF encoding can be divided into five steps. (1) A set of $I$ desired, ideal, complex $B_1$-gradients $B_{1i}^{ideal}$ is defined ($i=1…I$). The gradients do not need to be constant, any gradient set leading to the required orthogonality is sufficient. (2) The sensitivities $S_n$ of the $N$ transmit array elements ($n=1…N$) of the multi-channel MR system are measured using the phantom / subject under investigation. (3) The desired gradients are approximated by an optimized superposition of the measured sensitivities. The optimization can be performed via linear algebra based on

$$B_{1i}^{ideal}(\vec{x}) = \sum_{n \leq N} W_{ni} S_n(\vec{x}) \cdot \tag{1}$$

This leads to a list of complex weighting coefficients $W_{ni}$ for each transmit element $n$ and each encoding step $i$. (4) The scan is performed while stepping through the previously calculated $B_1$-field configurations, applying the weighting coefficients to the individual RF channels, which are driving the corresponding transmit elements. For each step, a single data point is measured during the FID, filling a "pseudo k-space"

$$D_i \sim \int_{volume} M(\vec{x}) \frac{B_{1i}(\vec{x})}{|B_{1i}(\vec{x})|} \sin(\gamma\tau |B_{1i}(\vec{x})|) dV \cdot \tag{2}$$

with $M$ the signal density including relaxation effects, $D_i$ the complex data point, $\tau$ the effective RF pulse duration, and $\gamma$ the gyromagnetic ratio. Signal reception via a homogeneous body coil is assumed. The structure of Eq. (2) reflects the sinus modulation of the applied $B_1$-field during RF transmission, which affects only the amplitude $|B_1|$, but not the phase $B_1/|B_1|$. (5) Image reconstruction from this pseudo-k-space is performed, e.g., via matrix inversion of the discretized Eq. (2)

$$\underline{D} = \underline{\underline{E}} \underline{M} \tag{3}$$

with $\underline{D}$ a vector containing the $I$ measured values, $\underline{M}$ containing the values of $M$ discretized on a spatial grid of $J$ pixels, and $\underline{\underline{E}}$ the $J{\times}I$ encoding matrix (see Eq. (2))

$$E_{ji} = \frac{B_{1i}(\vec{x}_j)}{|B_{1i}(\vec{x}_j)|} \sin(\gamma\tau |B_{1i}(\vec{x}_j)|) \cdot \tag{4}$$

Finally, the desired distribution $\underline{M}$ can be reconstructed via solving Eq. (3) (the (regularized) pseudo-inverse [5] denoted by +)

$$\underline{M} = \underline{\underline{E}}^+ \underline{D} \cdot \tag{5}$$

***Methods:***
Experiments were performed on a 3T Philips Achieva (Philips Medical Systems, Best, The Netherlands) extended with eight independent transmit channels [4]. The Tx/Rx body coil consists of eight cylindrically arranged elements [6]. The chosen ideal $B_1$-gradients were kept constant in phase and amplitude. To achieve a spatial resolution of $J = 16{\times}16$ pixels, $I = 256$ data points were acquired. For each of the 16 different radial directions, 2 different phase slopes and 8 different amplitude slopes were applied, thus yielding $I = 256$ data points in total. To check for the individual sensitivities, not only a single data point was measured per $B_1$-gradient, but a low-resolution image (FFE, TE/TR=4/25ms, grid size = 16²). The central k-space point of the low-resolution image was taken for the pseudo-k-space. A cylindrical quality oil phantom was used ($\varnothing = 25$ cm, length = 20 cm) for experimental validation.

***Results:***
Figure 1 compares an ideal $B_1$-gradient with the real gradient. Both gradients show sufficient agreement as indicated by a 93.3% correlation. Figure 2 shows three low-resolution examples of RF encoded phantom images. Figure 3 shows the corresponding images acquired with standard $B_0$-encoding. The correlation between Fig. 2 and Fig. 3 is 92.9 / 74.1 / 76.7% for the three examples.

***Discussion/Conclusion:***
A recently developed multi-transmit MR system allows testing the well-known idea of RF encoding via $B_1$-gradients into multiple spatial dimensions. In the framework of the described initial experiments, the basic feasibility of image reconstruction via RF encoding was demonstrated. The chosen mathematical approach allows also the handling of non-ideal $B_1$-gradients, as long as the resulting encoding matrix is well-posed. The study concentrates on in-plane encoding exclusively via $B_1$-gradients. However, also a mixture of applying $B_0$ and $B_1$-gradients is possible. Furthermore, future studies have to investigate the possibility to increase the spatial resolution, the reduction of the scan time, and the associated SAR. In any case, RF encoding offers the potential of reducing acoustic noise, of reducing the $B_0$-gradient amplifier requirements and of reducing the sensitivity to susceptibility effects.
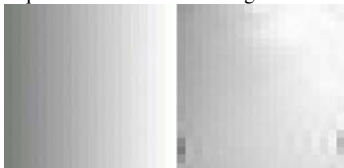


Fig. 1: Example of a desired, ideal B1 gradient (amplitude, left) and the corresponding real gradient (right).
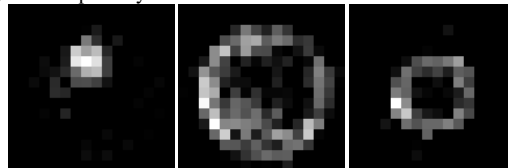


Fig. 2: Three example images of a phantom measured via B1 gradients.
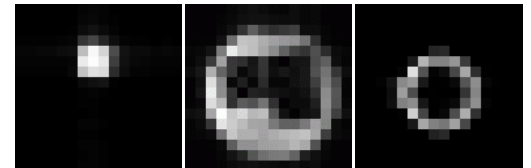


Fig. 3: Same images as in Fig. 2, but measured via standard B0 gradients.

***References:***
[1] D.I. Hoult, JMR 33 (1979) 183, [2] A.A. Maudsley, MRM 3 (1986) 768, [3] G.S. Karczmar et al., MRM 7 (1988) 111, [4] I. Graesslin et al., ISMRM 14 (2006) 129, [5] A. Tarantola, "Inverse Problem Theory", Elsevier Amsterdam, 1987, [6] P. Vernickel et al., ISMRM 14 (2006) 123